



Article

Parameter Sensitivity Analysis for Long-Term Nuclide Migration in Granite Barriers Considering a 3D Discrete Fracture–Matrix System

Yingtao Hu ^{1,2,3} , Wenjie Xu ^{3,*} , Ruiqi Chen ³, Liangtong Zhan ³, Shenbo He ⁴ and Zhi Ding ^{1,2}

¹ School of Engineering, Hangzhou City University, Hangzhou 310015, China; huyt@hzcu.edu.cn (Y.H.); dingz@hzcu.edu.cn (Z.D.)

² Key Laboratory of Safe Construction and Intelligent Maintenance for Urban Shield Tunnels of Zhejiang Province, Hangzhou City University, Hangzhou 310015, China

³ MOE Key Laboratory of Soft Soils and Geoenvironmental Engineering, Zhejiang University, Hangzhou 310058, China; cricky_zju@163.com (R.C.); zhanlt@zju.edu.cn (L.Z.)

⁴ School of Civil Engineering and Architecture, Guangxi University, Nanning 530004, China; shenbohe@st.gxu.edu.cn

* Correspondence: wenjiexu@zju.edu.cn

Abstract: As a geological barrier for high-level radioactive waste (HLW) disposal in China, granite is crucial for blocking nuclide migration into the biosphere. However, the high uncertainty associated with the 3D geological system, such as the stochastic discrete fracture networks in granite, significantly impedes practical safety assessments of HLW disposal. This study proposes a Monte Carlo simulation (MCS)-based simulation framework for evaluating the long-term barrier performance of nuclide migration in fractured rocks. Statistical data on fracture geometric parameters, on-site hydrogeological conditions, and relevant migration parameters are obtained from a research site in Northwestern China. The simulation models consider the migration of three key nuclides, Cs-135, Se-79, and Zr-93, in fractured granite, with mechanisms including adsorption, advection, diffusion, dispersion, and decay considered as factors. Subsequently, sixty MCS realizations are performed to conduct a sensitivity analysis using the open-source software OpenGeoSys-5 (OGS-5). The results reveal the maximum and minimum values of the nuclide breakthrough time T_t (12,000 and 3600 years, respectively) and the maximum and minimum values of the nuclide breakthrough concentration C_{max} (4.26×10^{-4} mSv/a and 2.64×10^{-5} mSv/a, respectively). These significant differences underscore the significant effect of the uncertainty in the discrete fracture network model on long-term barrier performance. After the failure of the waste tank (1000 years), nuclides are estimated to reach the outlet boundary 6480 years later. The individual effective dose in the biosphere initially increases and then decreases, reaching a peak value of $C_{max} = 4.26 \times 10^{-4}$ mSv/a around 350,000 years, which is below the critical dose of 0.01 mSv/a. These sensitivity analysis results concerning nuclide migration in discrete fractured granite can enhance the simulation and prediction accuracy for risk evaluation of HLW disposal.

Keywords: risk evaluation; nuclide migration; long-term performance; discrete fracture–matrix system; Monte Carlo simulation



Citation: Hu, Y.; Xu, W.; Chen, R.; Zhan, L.; He, S.; Ding, Z. Parameter Sensitivity Analysis for Long-Term Nuclide Migration in Granite Barriers Considering a 3D Discrete Fracture–Matrix System. *Fractal Fract.* **2024**, *8*, 303. <https://doi.org/10.3390/fractalfract8060303>

Received: 2 April 2024

Revised: 16 May 2024

Accepted: 17 May 2024

Published: 21 May 2024



Copyright: © 2024 by the authors. Licensee MDPI, Basel, Switzerland. This article is an open access article distributed under the terms and conditions of the Creative Commons Attribution (CC BY) license (<https://creativecommons.org/licenses/by/4.0/>).

1. Introduction

Nuclear energy holds vast potential as a low-carbon energy source [1,2]. However, reprocessing spent fuel produces high-level radioactive waste (HLW), characterized by potent radioactivity, extreme toxicity, and a prolonged half-life. Any leakage of this waste could precipitate severe environmental repercussions and pose significant threats to human health. Currently, deep geological disposal, often designed based on multi-barrier systems comprising engineered and geological barriers, is considered a technically feasible and

safe method for the long-term management of HLW [3,4]. These multi-barrier systems, illustrated in Figure 1, are aimed at preventing or delaying the movements of nuclides into the biosphere, reducing environmental impacts to an acceptable level, and achieving long-term safe isolation exceeding 10,000 years. Crystalline or granitic rock, known for its geological stability, low permeability, and desirable mechanical properties, is extensively recognized as a suitable host rock for HLW disposal repositories in countries such as Sweden, Switzerland, Finland, and China, among others. Nonetheless, granite as a fractured porous medium harbors fractures that can potentially serve as potential pathways for groundwater flow, allowing nuclide transport into the biosphere and ultimately compromising the service life of the repository. Thus, accurate characterization of the long-term nuclide migration properties in fractured rocks and precise prediction of their transport processes hold significance for assessing the long-term barrier performance and safety assessment of HLW disposal repositories.

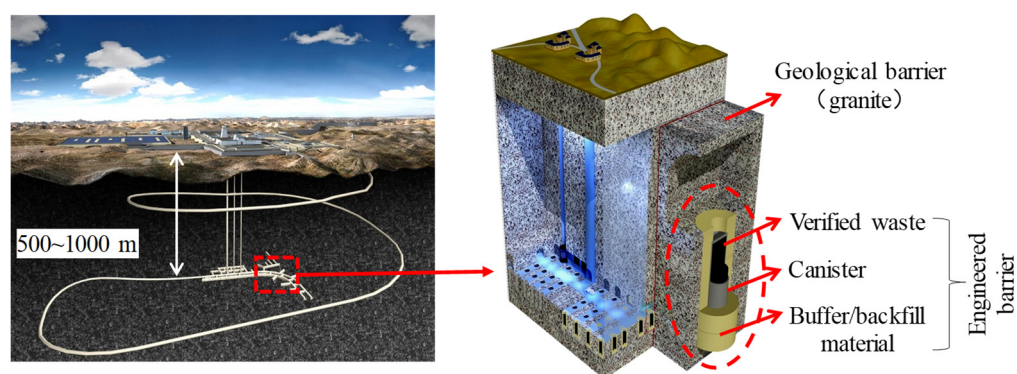


Figure 1. Multi-barrier systems for HLW repository [4,5].

Concerning the long-term barrier performance assessment of fractured geological barriers, extensive studies have been conducted on the flow and transport characteristics of nuclides in fractured rocks. These studies include field and laboratory tests [6,7], such as in situ drilling tracer and underground research laboratory (URL) nuclide migration tests [8–11], theoretical analyses [12–14], and numerical simulations [15–18]. In situ tracer tests using non-sorbing and sorbing tracers were conducted at the Äspö site in Sweden from 1995 to 2005 to understand nuclide migration and retention processes in fractured rocks [8,19,20]. Similarly, large-scale in situ tracer tests were performed at the Forsmark candidate area for a deep repository in Sweden to investigate the connectivity between water-bearing structures and their transport properties [9,21]. Soler et al. [10] and Ikonen et al. [22] performed long-term in situ diffusion experiments spanning two years at the Grimsel Test Site (GTS) in Switzerland. They found significant diffusion of the tracers into the granitic matrix. Tanaka et al. [11] carried out in situ tracer tests at the Mizunami URL in Japan to determine the transport properties of the rock mass and develop evaluation methods for crystalline rock. These in situ tracer tests provide crucial information on transport parameters (such as the length of the flow path, flow velocity, and longitudinal dispersivity) and retention parameters (retardation factors) for predicting long-term nuclide migration. However, identifying potential pathways in geological barriers and inferring long-term nuclide migration over thousands of years from in situ tracer experiments remain a challenge.

Numerical modeling, coupled with in situ tracer tests and laboratory experiments, provides insights into the long-term performance of disposal repositories [7]. Several simulations have recently been performed to characterize the long-term barrier performance of HLW disposal repositories [13,17,23,24]. Ling et al. [23] employed GoldSim software (<https://www.goldsim.com/>) to simulate nuclide migration and assess the effectiveness of a geological barrier at the Beishan repository in China, focusing on the 1000 years post-closure of the repository. Duan et al. [24] used Monte Carlo simulation to model

structural damage and estimate radiation levels over 1 million years following the closure of the disposal repository. Jia et al. [13] proposed a simulation framework to quantify uncertainty in nuclide migration associated with HLW disposal. They conducted statistical analysis and global sensitivity assessments by integrating the nuclide migration simulator FRACPIPE with the uncertainty quantification tool PSUADE. These studies simulated the interactions and dependencies between repository subsystems and nuclide transport through engineered and geological barriers, simplifying the barrier into a one-dimensional model for fractured media. Nonetheless, these studies did not consider stochastic discrete fracture networks, which govern the realistic behaviors of groundwater flow and nuclide migration within geological barriers, including their geometries, connectivity, and hydraulic properties.

The discrete fracture network (DFN) method is extensively used in modeling fractured rocks because of its ability to explicitly represent discrete fractures [25–28]. This approach has also been widely used to predict long-term nuclide migration in fractured rocks. Posiva, the Finnish nuclear waste disposal company, established a three-dimensional (3D) DFN model based on the in situ geometric parameters of fractures to calculate the nuclide migration paths in repositories using the ConnectFlow code [29]. Using the dfn-Works framework, Hyman et al. [30] investigated the evolution of the solute transport properties in a kilometer-scale 3D DFN for the SKB (Swedish Nuclear Fuel and Waste Management Company) site in Forsmark, Sweden. Wei et al. [17] combined the DFN model and probabilistic distribution to evaluate the risk of nuclear waste disposal in China and analyze areas with probabilities of contamination. While it accurately captures the geometric and topological characteristics of fracture networks, the DFN model may not be directly suitable for problems involving interactions between fracture networks and the surrounding rock matrix [31–33]. This constraint may be addressed using the discrete fracture–matrix (DFM) model. This model enables direct simulation of the solute exchange at the interface between fractures and the rock matrix, allowing for a more comprehensive analysis of solute transport in fracture–matrix systems, and has been widely employed to analyze solute migration in fractured rocks [34–37]. Ben Abdelghani et al. [38] used the HydroGeoSphere model to explore the mechanism by which conductivity and fracture network properties influence contaminant transport in unsaturated water flow within fractured rock characterized by orthogonal fracture networks. Ma et al. [18] proposed the unified pipe–network method to simulate and analyze nuclide migration in highly fractured rocks with complex fracture networks. Hu et al. [37] and Hyman et al. [39] developed an efficient numerical simulation workflow for investigating problems in fractured porous media using the discrete fracture–matrix approach. Using the multiscale fracture integrated equivalent porous medium method, which uniformly characterizes multiscale fractures (large-, medium-, and small-scale fractures) and the rock matrix, Ma et al. [40] simulated the fluid flow and solute transport in a multiscale fracture–matrix system. The aforementioned studies emphasize the potency of the DFM model in simulating complex heterogeneous fractured media. Although the DFM model has provided valuable insights into the fluid flow and solute transport in fractured rocks, a critical gap remains in our understanding of the long-term barrier performance of repositories, particularly when considering stochastic DFM systems. Numerical simulation based on DFM models offers a feasible approach for predicting nuclide migration in fractured granite. By incorporating the effects of matrix diffusion, this model can provide valuable insights into the long-term behavior of nuclides in geological barriers, thus improving the safety assessment of HLW disposal.

Motivated by the aforementioned unresolved concerns, this study aims to analyze the nuclide migration behavior and evaluate the long-term efficacy of a granite barrier, considering a stochastic discrete fracture–matrix system. This paper is organized as follows: A simulation framework is proposed for evaluating the long-term barrier performance of nuclide migration in a 3D discrete fracture–matrix system by using Monte Carlo simulation (MCS) in Section 2. Statistical data regarding the fracture geometric parameters, on-site hydrogeological conditions, and relevant migration parameters obtained from the research

site in Northwestern China are presented. In Section 3, sixty 3D DFM realizations are performed using the open-source software OpenGeoSys-5 (OGS-5). These simulations investigate the migration of three key nuclides—namely Cs-135, Se-79, and Zr-93—within fractured granite. Several mechanisms are considered: adsorption, advection, diffusion, dispersion, and decay. Section 4 discusses the sensitivity analysis of the nuclide breakthrough time T_t and nuclide breakthrough concentration C_{max} . These analyses are intended to elucidate nuclide migration behaviors and predict the long-term performance of the granite barrier for HLW disposal.

2. Methodology

2.1. Monte Carlo Simulation

Figure 2 illustrates the MCS procedures for assessing the long-term performance of a granite barrier. First, the input parameters, including the geometric indicators of the research object (length, width, depth) and fractures (fracture orientation, length, and density), the key nuclides, physical considerations, and hydrogeological conditions, are obtained. Numerous 3D DFM models are then generated based on the geometric parameters of fractures by using Monte Carlo simulation. Appropriate theoretical analytical models relevant to the study area are chosen, including the rock matrix–fracture interaction, sorption phenomena, and decay processes. Moreover, OGS calculations for N cases of 3D DFM models are performed to determine the flow and concentration fields, breakthrough curves (BTCs), breakthrough time (T_t), and maximum breakthrough concentration (C_{max}). Finally, a statistical analysis of the output T_t and C_{max} is conducted to estimate the long-term geological barrier performance of the HLW repository.

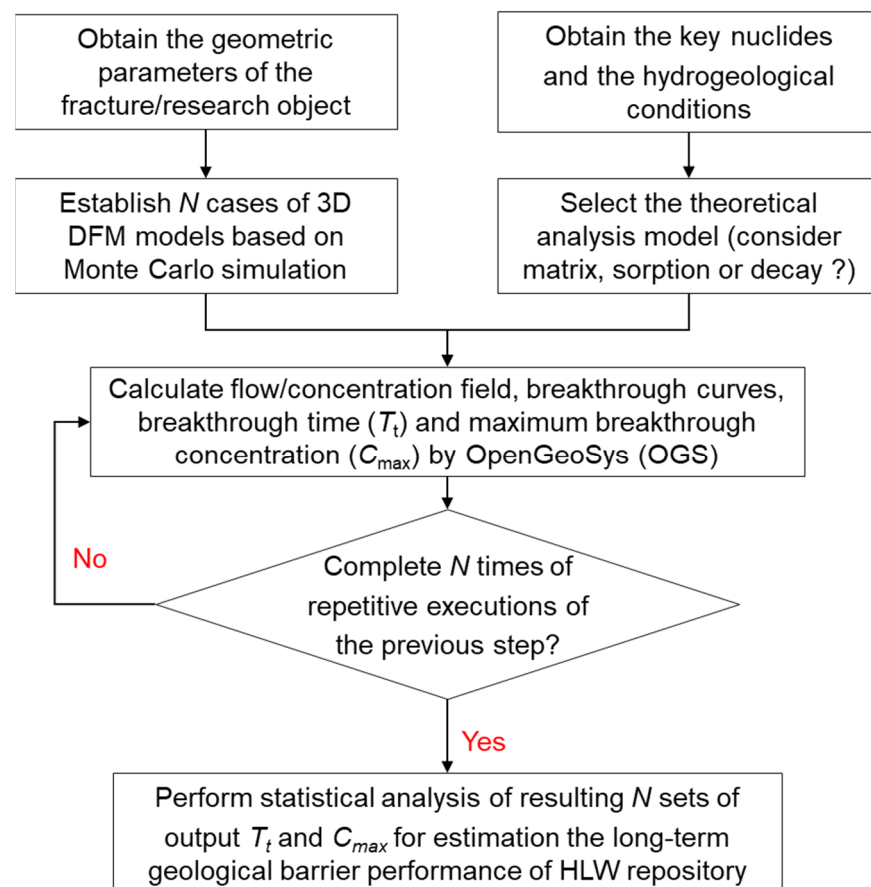


Figure 2. Monte Carlo simulation of the long-term barrier performance of granite barrier.

2.2. The Three-Dimensional Discrete Fracture–Matrix System

Figure 3 presents the main components of and a conceptual model of nuclide migration in a hypothetical scenario of HLW disposal. The minimum distances from the disposal pit to the water-conducting fractures, water-conducting faults, and rock boundaries are 10, 100, and 1000 m, respectively, as previously reported by Chen et al. [41]. In the current study, the focus is on the geological barrier encompassing the water-conducting fractures (denoted in red in Figure 3). This barrier represents a typical discrete fracture–matrix system. In this system, the following assumptions were made:

- (1) The convection, molecular diffusion, adsorption, and decay mechanisms of the nuclides in the fractured rock are considered.
- (2) The scenario assumes the failure of the containers and buffer materials within a disposal pit 1000 years post-closure of the disposal facility. Thus, the disposal pit is directly connected to the water-conducting fractures, causing nuclide leakage into the fractured granite barrier under groundwater flows.
- (3) The water-conducting fractures in the geological barrier exhibit a stochastic distribution owing to the difficulty of identifying all the fracture geometries at the disposal site. In the following simulation, the water-conducting fracture zones are represented by a discrete fracture–matrix system with scale of 100 m.
- (4) The distances of the disposal pits to the water-conducting fractures varied because the disposal pits were aligned with the disposal facility. For simplicity, we consider the nearest disposal pit, 20 m high and 2 m wide, as the pollution source.

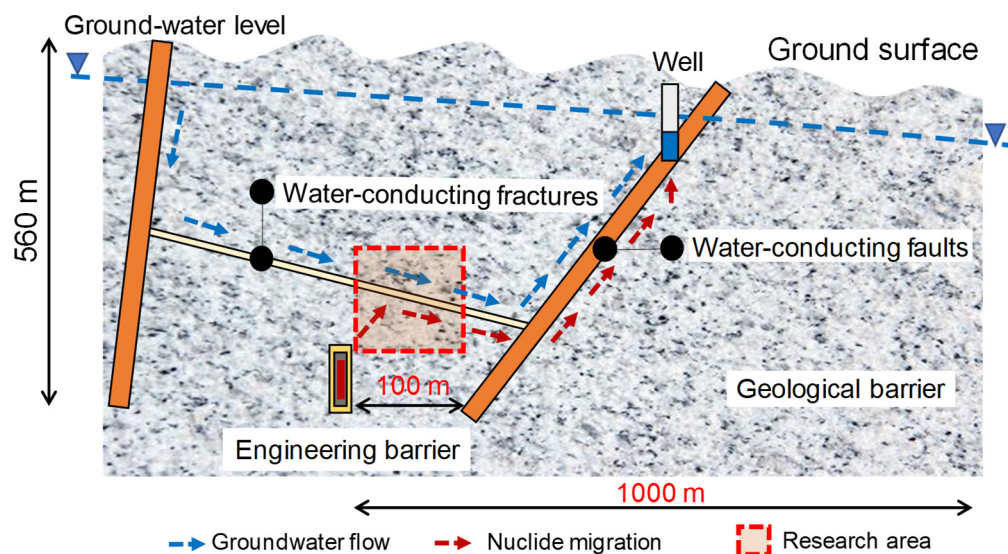


Figure 3. Conceptual model of nuclide migration in the HLW disposal.

In recent decades, extensive field surveys have been conducted in various preselected regions in the Beishan area of China [4,42–44]. These studies have yielded geometric parameters of the fractures, including their orientation, trace length, and density, measured on site. With these parameters, a DFN model can be randomly generated using MCS. For more complex fracture systems, it is shown that power laws and fractal geometry provide widely applicable tools to describe fracture networks [45–47]. Specifically, power-law scaling has been applied to characterize trace length, spatial distribution, fracture aperture, fracture roughness, etc., that influence the connectivity of fractured rocks. In the current study, the DFN models are represented by circular disks within a cubic domain, and the geometric parameters of the fractures, such as fracture orientation, dip angle, and density, as reported by Xu et al. [44], are listed in Table 1a. The fracture orientation (dip direction and dip angle) follows a Fisher distribution according to Xu et al. [44], whereas the fracture center location and density are assumed to have a uniform distribution. It should be

noted that the statistical results on the mean fracture length/size in the Beishan area vary greatly [44,48,49], as summarized in Table 1b. To optimize subsequent simulations and achieve a balance between the computational power and calculation efficiency, this study used the data obtained by Lei et al. [48]. Based on their study, the fracture length/size follows a normal distribution, and the mean fracture length/size and standard deviation were assumed to be 20 m and 10 m, respectively. In addition, when constructing the DFN models, the stop condition for generating fractures in the domain was controlled by giving a total number of fractures to constrain the final number of fractures in the matrix instead of a density index, and to guarantee the generation of the four fractures sets, probability, which was calculated according to the ratio of the number of each set to the total number of the four sets, was used to generate the final DFN models.

Table 1. (a) Parameters of fracture sets at the Beishan site in China [44]. (b) The mean fracture length/size at the Beishan site in China [44,48,49].

| (a) | | | | | |
|---------------------------|-------------------|----------------|----------------------------|--------|-------------|
| Set | Dip Direction (°) | Dip Angle (°) | <i>k</i> (Fisher Constant) | Number | Probability |
| 1 | 79.2 | 60.3 | 19.05 | 52 | 0.347 |
| 2 | 330.9 | 24.9 | 23.32 | 30 | 0.200 |
| 3 | 286.3 | 75.8 | 33.96 | 38 | 0.254 |
| 4 | 250.5 | 73.6 | 15.86 | 30 | 0.200 |
| (b) | | | | | |
| References | Lei [48] | Xu et al. [44] | Li [49] | | |
| Mean fracture length/size | 17.08–22.20 | 2.798–5.883 | 0.345–1.178 | | |

To maintain generality and conduct a sensitivity analysis of the nuclide migration characteristics within the water-conducting fracture zones, 60 independent 3D DFM realizations with different geometries were established using the open-source tool *dfnWorks* [30] based on the parameters in Table 1a. These realization numbers are consistent with our previous work [50], which are enough to demonstrate the nuclide migration results. Furthermore, the fracture aperture was defined in relation to the fracture size with a power-law relationship of $b = 5.0 \times 10^{-4} \sqrt{r}$, which is a widely used relationship, as reported in Bonnet et al. [45] and Hyman et al. [51]. Therefore, the fracture aperture varies among the DFNs, with larger fractures having wider hydraulic apertures than the smaller fractures. Figure 4 presents a realization of the 3D DFM model, together with the corresponding meshing result. The model depicts a cubic domain with a side length of 100 m; variations in the fracture color represent differences in the fracture apertures, with the color intensity reflecting the size of the aperture.

It should be noted that the relationship between the nuclide migration characteristics and the connectivity of the fracture network structures, such as the percolation probability and geological entropy, is an important issue for studying nuclide migration in fracture–matrix systems. However, for each DFM realization generated in this study, the fractures intersected with at least one other fracture, and the DFM consisted of at least one connected flow channel with fractures connecting the inlet and outlet surfaces. Equally, isolated fractures that did not intersect with any other fracture and would not contribute to the flow were removed after the DFM was generated. Therefore, all the final DFM models studied in this paper were percolation models.

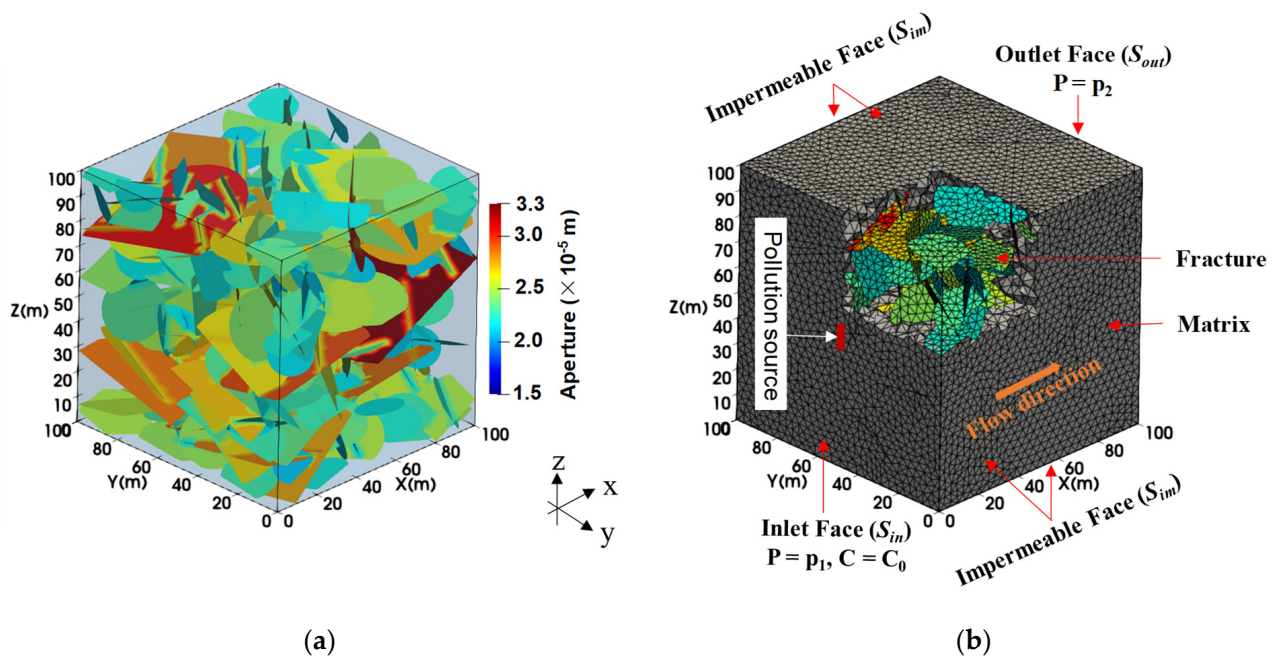


Figure 4. (a) Three-dimensional discrete fracture matrix model and (b) corresponding meshes.

2.3. Flow and Transport Equations

The governing equations in this study include fluid flow and mass transport in fractured and porous media [52,53]. For saturated rock fractures, the mass balance equation for laminar fluid flow can be expressed as

$$bS_f \frac{\partial P}{\partial t} + \nabla \cdot b\mathbf{u}_f = 0 \quad (1)$$

where S_f is the storage coefficient of the fractures (1/Pa), P is the water pressure, ρ_w is the water density, g is the gravitational acceleration, H is the hydraulic head, and \mathbf{u}_f is Darcy's velocity in the fractures (m/s), which can be calculated according to the cubic law

$$\mathbf{u}_f = -\frac{b^2}{12\mu}(\nabla P + \rho_w \mathbf{g}) \quad (2)$$

where μ is the dynamic viscosity.

For the fluid flow in the rock matrix, which is a porous medium, the mass balance equation can be expressed as

$$S_m \frac{\partial P}{\partial t} + \nabla \cdot \mathbf{u}_m = 0 \quad (3)$$

where S_m is the storage coefficient of the rock matrix (1/Pa), and \mathbf{u}_m is Darcy's velocity in the rock matrix (m/s), which is given by

$$\mathbf{u}_f = -\frac{\mathbf{K}}{\mu}(\nabla P + \rho_w \mathbf{g}) \quad (4)$$

where \mathbf{K} is the permeability (tensor) of the porous medium (m^2).

The parameters in Equations (2)–(4) are listed in Table 2a. As for our saturated flow simulation, the storage coefficients of the fractures and the rock matrix are set to 1 (1/Pa).

Table 2. (a) Parameters for Equations (2)–(4) in the 3D DFM simulations. (b) Parameter definition in Equation (5).

| (a) | | | |
|--------------|-------------------------------------|-------------------------|-------------------------|
| Symbol | Parameter | Value | Unit |
| S_f | Storage coefficient of fractures | 1 | 1/Pa |
| S_m | Storage coefficient of rock matrix | 1 | 1/Pa |
| g | Gravitational acceleration | 9.8 | kg/m ³ |
| ρ_w | Water density | 1000 | kg/m ³ |
| μ | Dynamic viscosity | 1×10^{-3} | Pa s |
| (b) | | | |
| Symbol | Parameter | Fractures ($\pi = f$) | Matrix ($\pi = m$) |
| C_π | Concentration | C_f | C_m |
| θ_π | Porosity | 1 | θ |
| τ_π | Tortuosity | 1 | τ |
| u_π | Velocity | u_f | u_m |
| D_h^π | Hydrodynamic dispersion coefficient | $\alpha_L u_f + D^*$ | τD^* |
| R_π | Retardation coefficient | $1 + 2K_f/b$ | $1 + \rho_b K_m/\theta$ |
| λ | Decay constant | | $\ln 2/t_{0.5}$ |

The nuclide transport through the discrete fracture–matrix system, as shown in Figures 3 and 4, can be calculated using the transport equation with source terms, given by

$$\frac{\partial \theta_\pi C_\pi}{\partial t} = \frac{1}{R_\pi} [\nabla \cdot \theta_\pi D_h^\pi (\nabla C_\pi) - \nabla \cdot (u_\pi C_\pi)] - \lambda \theta_\pi C_\pi \quad (5)$$

Definitions of the parameters in Equation (5) are listed in Table 2b, and the corresponding parameters for the simulations can be found in Table 4 in Section 2.4.1.

Notably, the hydrodynamic dispersion coefficient D_h^π considers the effects of effective molecular diffusion, $D_m^\pi = \tau_\pi D^*$, and mechanical dispersion, $D_d^\pi = \alpha_L^\pi u_\pi$. In addition, θ is the granite rock's porosity, τ represents the granite rock's tortuosity, ρ_b is the granite rock's density, D^* is the molecular diffusion coefficient in water, α_L is the longitudinal dispersivity, and $t_{0.5}$ is the half-life of the nuclides. K_f and K_m denote the distribution coefficients of the fracture and the rock matrix, respectively.

In the current study, the open-source finite element method software platform OGS was employed to solve the flow and transport equations. Nuclide exchange between the fractures and the matrix was achieved by coupling the conforming vertices at the fracture–matrix interface. Detailed verification of the numerical method is provided in our previous study [37].

2.4. Simulation Settings

2.4.1. Boundary and Hydrogeological Conditions

Figures 4b and 5 present the boundary conditions for the 3D DFM model. As shown in Figure 4b, the boundary conditions in the 3D DFM model consist of fixed water pressure at the inlet and outlet faces with $P|_{S_{in}} = p_1$ and $P|_{S_{out}} = p_2$, and no flow occurs at the other four faces, with $\mathbf{n} \cdot \nabla P|_{S_{im}} = 0$, where S_{in} , S_{out} , and S_{im} denote the inlet and outlet face and the four impermeable faces, respectively; \mathbf{n} represents the normal unit vector at the boundary surface. The pollution source is positioned at the center of the upstream or inlet face (S_{in}) for a clear observation of the nuclide migration in the geological barrier. Subsequently, the nuclides migrate in the fracture network channel under the hydraulic

gradients between the upstream and downstream water pressures. The evolution of the nuclide release rate downstream over time can then be calculated. Thus, the long-term performance of the geological barrier at a scale of 100 m can be evaluated and analyzed.

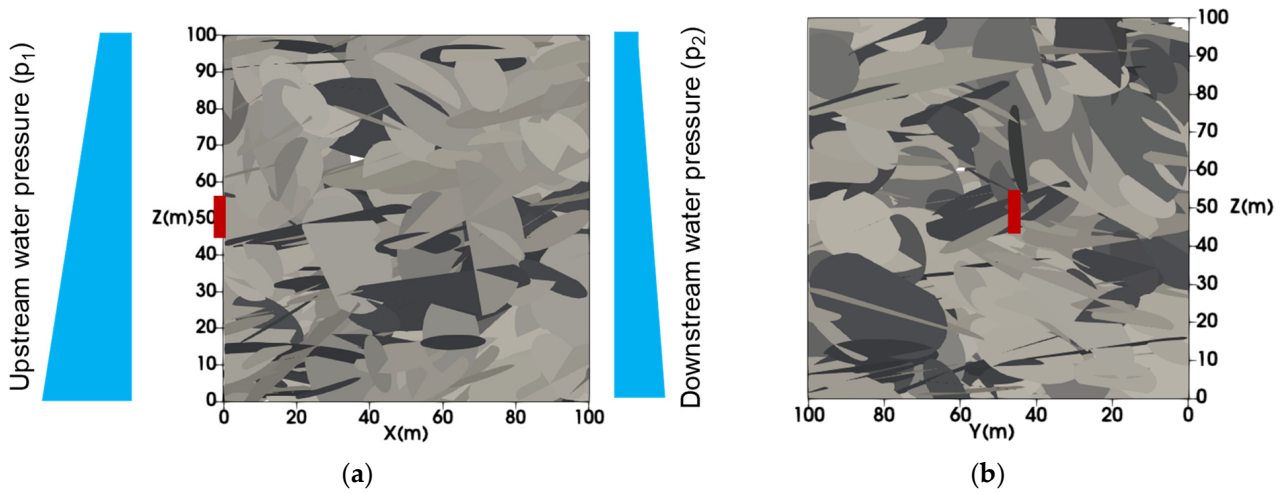


Figure 5. Boundary conditions of the 3D DFM models: (a) XZ direction; (b) YZ direction.

China is currently in the exploratory phase of studying the characteristics of spent fuel waste. Considering the similarities between spent fuel waste in China and Japan, this study mainly referred to the H12 report of the Japan Atomic Energy Commission when selecting key nuclides and relevant parameters [54]. According to the simulation results in the H12 report, the release rate of nuclides entering the biosphere is primarily attributed to the nuclides Cs-135, Se-79, and Zr-93 owing to their small distribution coefficient, high solubility, and strong migration ability. Thus, these three nuclides were selected as the key nuclides in our study. Figure 6 illustrates the release rates of the three key nuclides, Cs-135, Se-79, and Zr-93, from the engineering barrier system (EBS) using data from the H12 report, which lists the source concentrations at the inlet boundary. As shown in the graph, the release rates of Cs-135 and Zr-93 initially rise and then fall over time, whereas that of Se-79 gradually decreases over time.

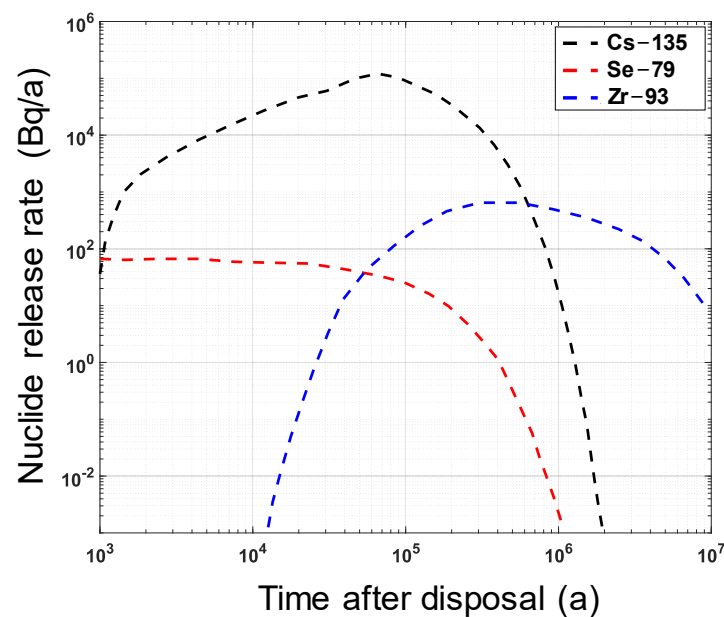


Figure 6. Release rates of key nuclides, Cs-135, Se-79 and Zr-93, at the boundary of the engineering barrier 1000 years post-closure of the repository (single waste package).

In addition, the migration characteristic parameters of Cs–135, Se–79, and Zr–93 are summarized in Table 3. These parameters include their half-lives, effective diffusion coefficients in granite, distribution coefficients, and dose coefficients. The main pathway by which nuclides could enter the human body from the disposal repository is ingestion; with this factor considered, the ingestion dose coefficient from the International Commission on Radiological Protection was used as the dose coefficient.

Table 3. Parameters of key nuclides Cs–135, Se–79, and Zr–93 [54].

| Nuclide | Parameters of the Nuclides | | | Parameters of the Granite Mass | | |
|---------|-------------------------------|---|--------------------------------|---|--|---|
| | Half-Life $t_{0.5}$ (Year) | Decay Coefficient λ (year ⁻¹) | Dose Coefficient (Sv/Bq) | Diffusion Coefficient D^* (m ² /s) | Effective Diffusion Coefficient D_d (m ² /s) | Distribution Coefficient K (m ³ /kg) |
| Cs–135 | 2.30×10^6 | 9.56×10^{-15} | 2.69×10^{-14} | | | 0.05 |
| Se–79 | 6.50×10^4 | 3.38×10^{-13} | 8.9×10^{-14} | 1.5×10^{-9} | 3×10^{-12} | 0.01 |
| Zr–93 | 1.53×10^6 | 1.43×10^{-14} | 5.5×10^{-15} | | | 0.1 |

Table 4 lists the hydrogeological parameters, including the hydraulic gradient and physical characteristics, of granite rock [41,55]. The site investigations and permeability tests in the Beishan area, China, suggested that the hydraulic conductivity of granite rock in the section of interest (i.e., 400–600 m below the ground surface) is extremely low, ranging between 3.9×10^{-14} and 6.6×10^{-10} m/s (corresponding permeability, 3.9×10^{-21} and 6.6×10^{-17} m²). Consequently, a permeability value within this range was chosen in this study, and the permeability coefficient of granite was set to 8.3×10^{-20} m². Furthermore, to consider potential adverse factors affecting nuclide migration in the geological barrier, the hydraulic gradient was set to 1%.

Table 4. Hydrogeological conditions in the 3D DFM simulations [18,41,55].

| Symbol | Parameter | Value | Unit |
|----------|-------------------------------------|---|-------------------|
| J | Hydraulic gradient | 0.1%~1% | - |
| K | Permeability coefficient of granite | 3.9×10^{-21} ~ 6.6×10^{-17} | m ² |
| θ | Porosity of granite | 0.58 | - |
| ρ_b | Density of granite | 2670 | kg/m ³ |
| τ | Tortuosity of granite | 0.1 | - |

2.4.2. Safety Assessment Considerations

In the present study, we propose two indicators for evaluating the long-term performance of the granite barrier [55]: (1) Time span: Safety and geological stability assessments from several countries, including Sweden, Finland, Japan, France, the United States, and Germany, suggest that the radiological risk significantly decreases over 1 million years, the maximum duration considered in these studies. Given this finding, we selected a simulation period of 1 million years and a reference time of 10 million years for our analysis of the peak release rates. (2) Safety metrics: Safety assessment indicators include the release rate and the effective dose. The release rate quantifies the rate of nuclide release in Bq/a during the same period. The effective dose represents the cumulative radiation dose (in mSv/a) received by an individual during a given period.

Table 5 lists the dose limits used by different countries in disposal safety assessments. The dose limit varies from 0.01 mSv/a to 0.25 mSv/a. In the current study, the minimum value (0.01 mSv/a) was selected as the dose limit, and the maximum effective dose, C_{max} , was considered for evaluating nuclide decay. The time at which the nuclide concentration

reaches C_{max} was defined as the decay time $t_{c, max}$. Therefore, based on the 100,000-year upper limit in safety assessments conducted by different countries, barrier failure or success was determined given the following conditions:

- (1) When $t_{c, max} \leq 100,000$ years, if $C_{max} \leq 0.01$ mSv/a, the barrier was deemed effective; otherwise, if $C_{max} > 0.01$ mSv/a, the barrier was deemed failed.
- (2) When $t_{c, max} > 100,000$ years, the barrier exceeded the upper limit and was deemed effective. Owing to the high toxicity and radioactivity of nuclides, they pose a significant threat to human life and health once they enter the biosphere. Accordingly, we defined the arrival time of the nuclides in the biosphere, T_t , as the moment when the effective dose is equal to 1.0×10^{-10} mSv/a. Thus, T_t was used to reflect the nuclide migration speed in the geological barrier.

Table 5. Dose limits used by different countries in disposal safety assessments [55].

| Country | Type of Geological Barrier | Safety Indicator | Limit Value (mSv/a) |
|---------------|----------------------------|------------------|-----------------------|
| Sweden | Granite | Dose | 0.014 |
| Finland | | | 0.1 |
| Japan | | | 0.01 |
| Canada | | | 0.3 |
| Switzerland | Claystone | Dose | 0.1 |
| France | | | 0.25 |
| Belgium | | | 0.1 |
| United States | Tuff | Dose | 0.15 (10,000 years) |
| Germany | Salt rock | | 1.0 (1,000,000 years) |
| | | | 0.01 |

3. Simulation Results

3.1. Flow Field

Figure 7 depicts the flow field distribution within the DFNs and the entire fracture–matrix system. Under a 1% hydraulic gradient, groundwater flows through the channels formed in the fracture network. The heterogeneity of the fracture networks leads to a significantly uneven distribution of the flow field, with a maximum flow velocity of 7.5×10^{-6} m/s and an average flow velocity of 7.46×10^{-7} m/s. The velocity within the rock mass approaches zero, which is attributed to the extremely low permeability of the granite rock (8.3×10^{-20} m²).

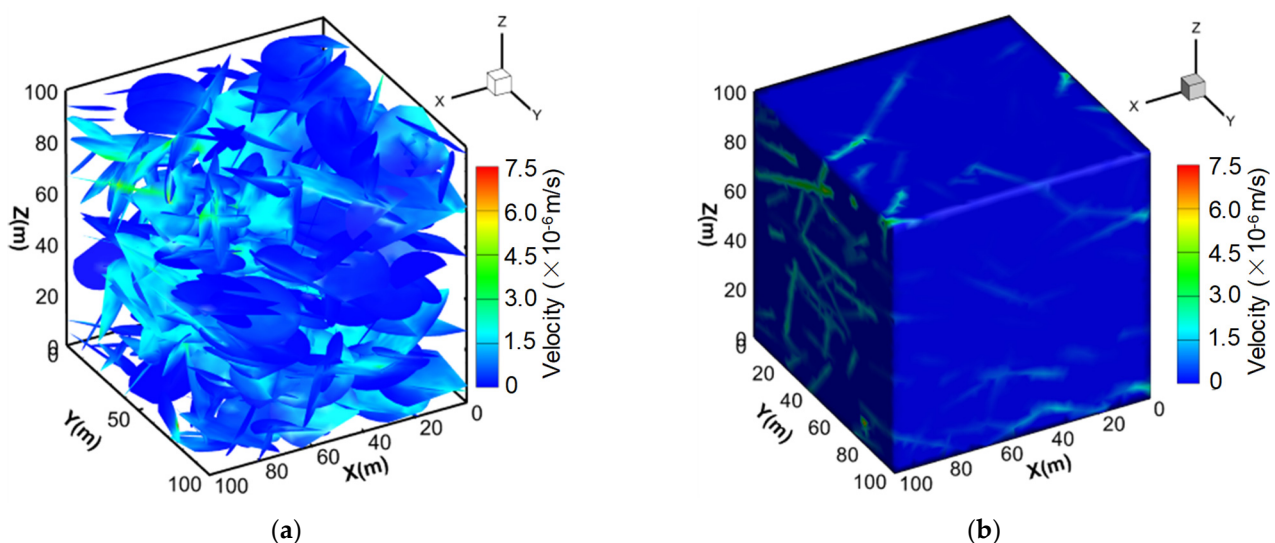


Figure 7. Flow field in the (a) DFNs and (b) entire discrete fracture–matrix system.

3.2. Evolution of the Concentration Field

To elucidate the evolutionary process of nuclide migration within the geological barrier, we selected a typical case from the 60 realizations. To clarify the detailed migration results inside the fractured rocks, the nuclide concentration distributions within both the DFNs and the rock matrix were separately examined, and the concentration distributions in the rock matrix were plotted according to a series of slices at $X = 0, 25, 50, 75,$ and 100 m, $Y = 50$ m, and $Z = 50$ m, respectively. Figures 8 and 9 present the migration results on the total nuclide release rates at different moments within the DFNs and the rock matrix (single waste package), respectively. As time progresses, the nuclides migrate within the fracture channels of the geological barrier in response to groundwater advection, molecular diffusion, and other occurrences. Simultaneously, these nuclides infiltrate into the surrounding granite matrix through matrix diffusion. This process widens the distribution range, ultimately reaching the outflow boundary of the geological barrier. However, the successive decay mechanism of Se-73, Cs-137, and Zr-93 prompts a decrease in the nuclide concentrations within the fracture channels after 500,000 years, further narrowing their distribution range.

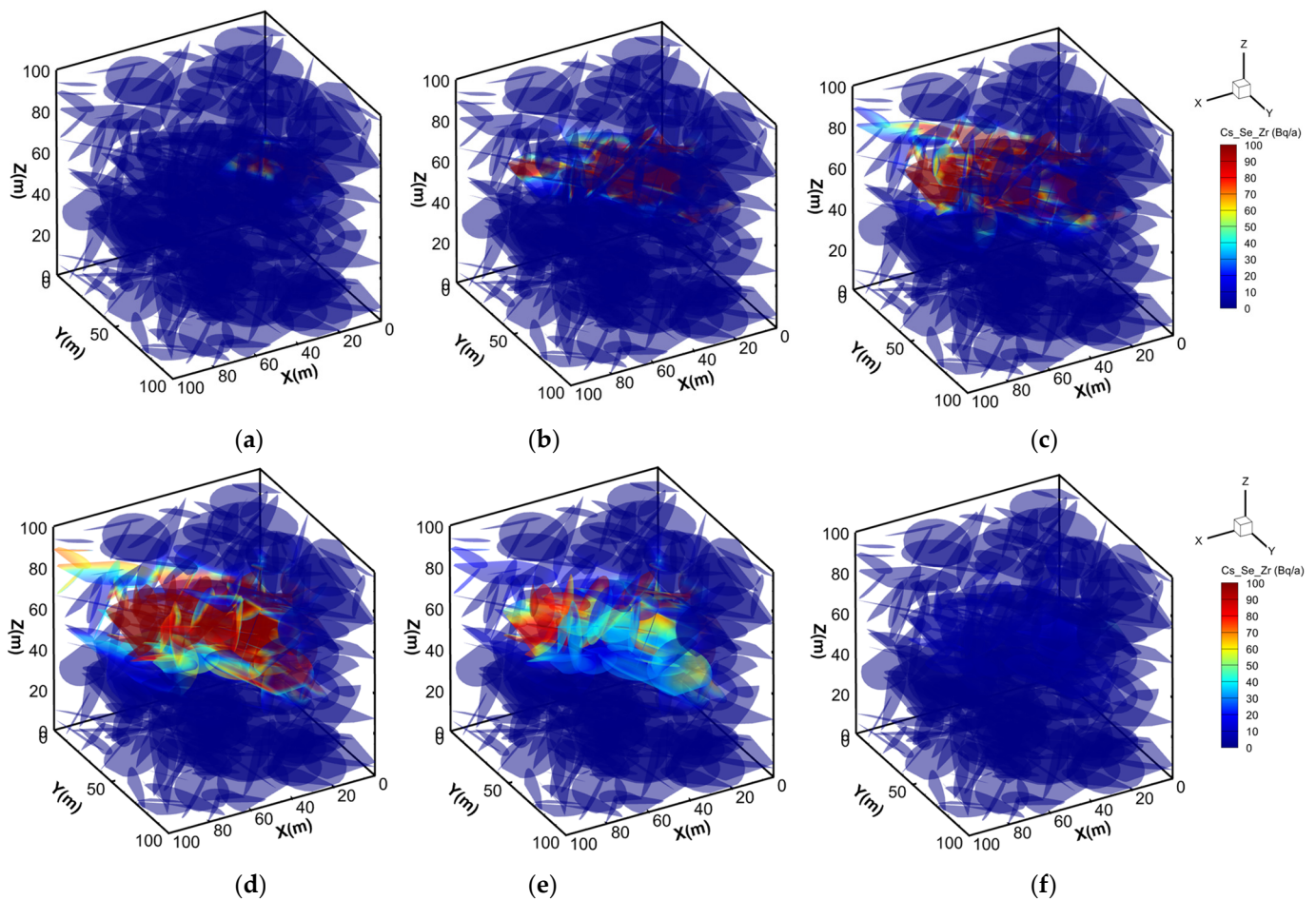


Figure 8. Distribution of total nuclide release rates (Bq/a) in DFNs at different moments 1000 years post-closure of the disposal repository (single waste package): (a) 10,000 years; (b) 50,000 years; (c) 100,000 years; (d) 500,000 years; (e) 1,000,000 years; (f) 5,000,000 years.

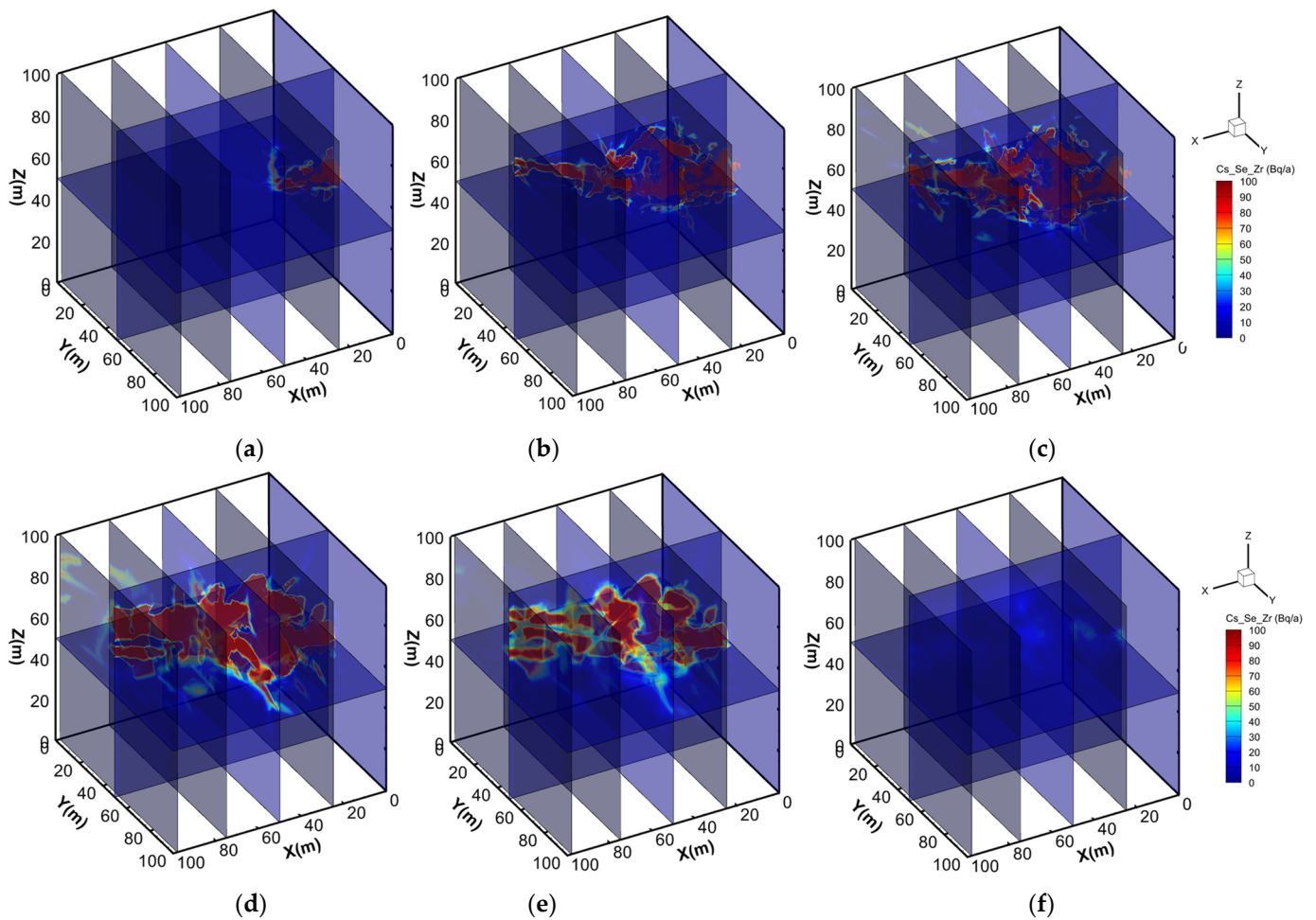


Figure 9. Distribution of total nuclide release rates (Bq/a) in the fracture–matrix system at different moments 1000 years post-closure of the disposal repository (single waste package): (a) 10,000 years; (b) 50,000 years; (c) 100,000 years; (d) 500,000 years; (e) 1,000,000 years; (f) 5,000,000 years.

3.3. Breakthrough Curves

Figure 10 shows the concentration breakthrough curves (BTCs) at the outflow boundary of the geological barrier for the key nuclides Cs–135, Se–79, and Zr–93, calculated from all 60 random realizations. The solid black line represents the cumulative concentration of the three nuclides. The BTCs exhibit variability due to the inherent uncertainty associated with the randomly distributed fracture network structures. Analyzing the average outflow BTCs from all the scenarios, we can conclude that the nuclides reach the boundary at approximately 7000 years (10^{-4} Bq/a) within 10 million years following the failure of the waste canister. Subsequently, the total nuclide release rate initially increases and then decreases, reaching a peak value of $C_{\max} = 51.6$ Bq/a at around 350,000 years. At 1 million years, the total nuclide release rate is 36.2 Bq/a. An analysis of the outflow concentrations of the three nuclides indicates that Se–73 is the earliest to exhibit a change in concentration. The total release rate of the nuclides in the initial stages is mainly attributed to Se–73 with its relatively strong migration ability (small retardation coefficient) and faster efflux rate. Owing to its markedly shorter half-life (65,000 years) than that of Cs–137 (2.3 million years), Se–73 begins to decay during migration over time, prompting a gradual decrease in its concentration. Meanwhile, the Cs–137 and Zr–93 concentrations gradually increase. As the migration time reaches the half-life of Cs–137 and Zr–93, the total release rates of these nuclides gradually decrease. When the Cs–137 concentration rises, its effect on the total release rate of the nuclides is predominant given its significantly higher source concentration compared with the other two nuclides (Figure 6).

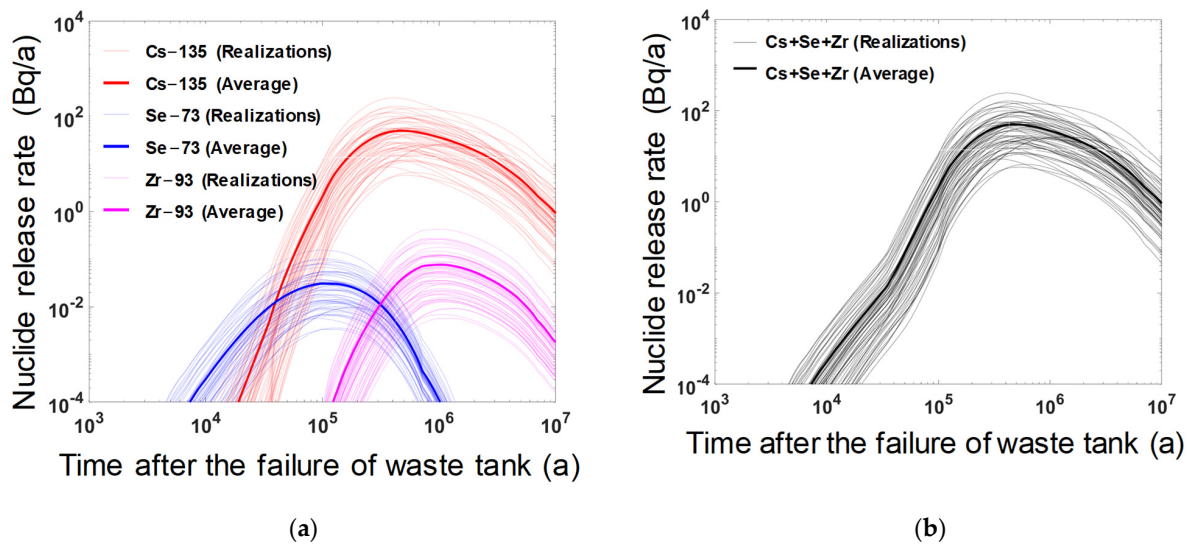


Figure 10. Breakthrough curves (BTCs) for all realizations at the outflow boundary 1000 years post-closure (single waste package): BTCs for (a) Cs–135, Se–79, and Zr–93, respectively; (b) cumulative BTCs of the three nuclides.

4. Discussion

4.1. Sensitivity Analysis of Breakthrough Time

In evaluating the long-term performance of the geological barrier in this study, the individual effective dose is analyzed, and the breakthrough time (T_t) and maximum breakthrough concentration (C_t) of the nuclides are evaluated. A total of 60,000 waste packages are estimated to be generated given the nuclear power development level of China in 2020 [55]. Under the extreme condition that all 60,000 waste packages break and release nuclides after 1000 years, the curve of the total individual effective dose over time can be calculated, as illustrated in Figure 11.

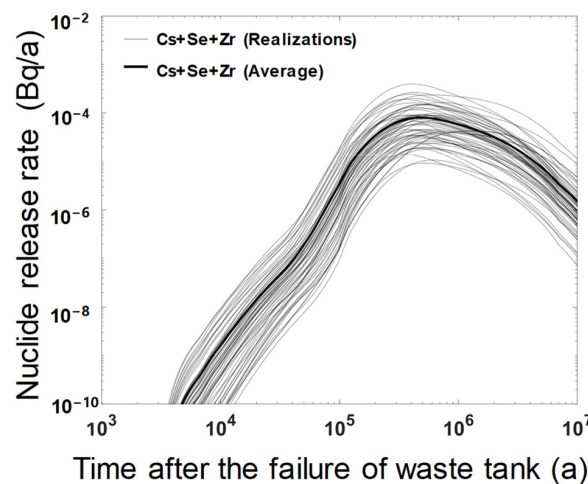


Figure 11. Breakthrough curves (BTCs) for the cumulative BTCs of nuclides Cs–135, Se–79, and Zr–93 1000 years post-closure for 60,000 waste packages.

Figure 12 illustrates the nuclide breakthrough time (T_t), together with a statistical histogram and cumulative probability density curve. As shown in Figure 12a, the maximum and minimum values of T_t are 12,000 and 3600 years, respectively, with a significant difference of 3.3 times. This significant difference emphasizes the noticeable effect of the uncertainty in the 3D DFM model on the breakthrough time results. As shown in Figure 12b, the breakthrough time of the nuclides obtained from the uncertainty analysis of the 3D DFM

models theoretically follows a normal distribution, with a mean and standard deviation of 6486 and 2412 years, respectively.

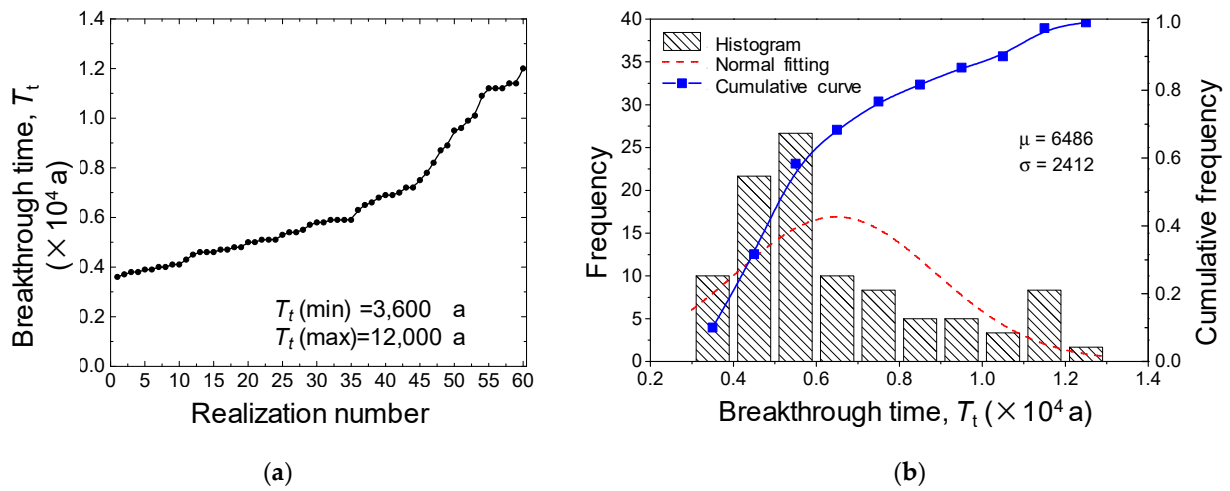


Figure 12. Uncertainty analysis of nuclide breakthrough time, T_t , based on random DFM models: (a) Calculation results of T_t ; (b) statistical histogram and cumulative probability density curve of T_t .

4.2. Sensitivity Analysis of Breakthrough Concentration

Figure 13 presents the maximum breakthrough concentration (C_{\max}) of the nuclides alongside a statistical histogram and cumulative probability distribution density curve. Figure 13a shows that the maximum and minimum values of C_{\max} are 4.26×10^{-4} and 2.64×10^{-5} mSv/a, respectively, with the former being 16.1 times greater than the latter, indicating a significant difference. As shown in Figure 13b, C_{\max} in all the realizations theoretically follows a normal distribution, with a mean and standard deviation of 7.84×10^{-5} and 6.04×10^{-5} mSv/a, respectively, indicating that the uncertainty of the DFM models significantly affects the maximum individual effective dose. This effect further influences the long-term performance of the geological barrier. These findings, combined with Figure 11, suggest that the individual effective dose reaches its peak state ($C_{\max} = 4.26 \times 10^{-4}$ mSv/a) at around 350,000 years, which falls below the dose limit of 0.01 mSv/a. This preliminary assessment indicates that the geological barrier at a scale of 100 m exhibits satisfactory long-term performance.

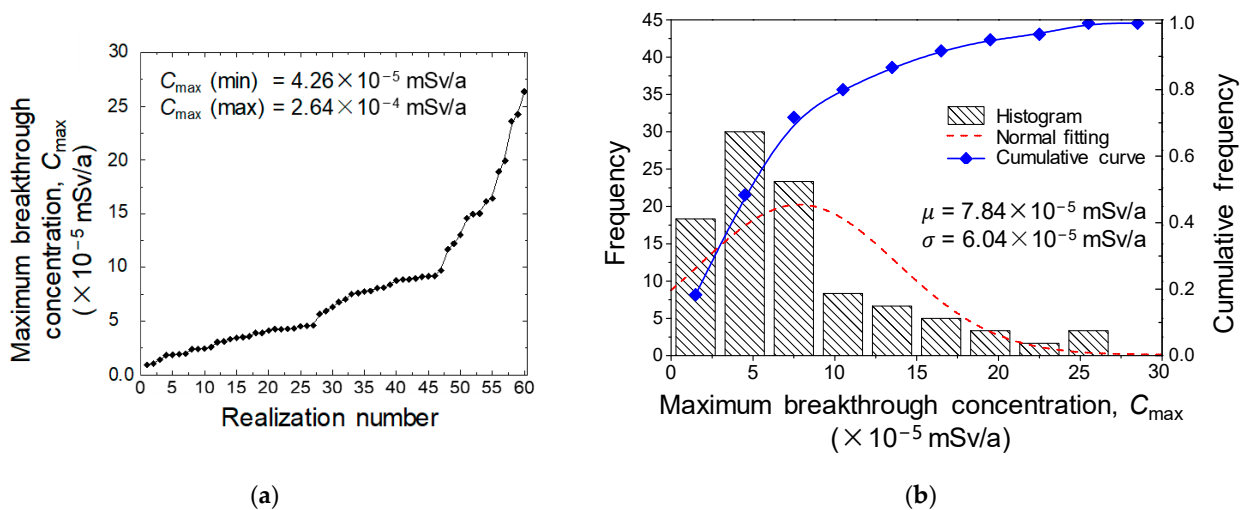


Figure 13. Uncertainty analysis of the nuclide breakthrough concentration C_{\max} based on the random DFM models: (a) calculation results for C_{\max} ; (b) statistical histogram and cumulative probability density curve of C_{\max} .

5. Conclusions

This study introduces a methodology for assessing the long-term barrier performance of low-permeability fractured rock masses using MCS and a 3D DFM model. The research focuses on a granite geological barrier designated for a proposed high-level radioactive waste (HLW) disposal repository in Northwestern China. It investigates the mechanism by which various parameters related to key nuclides—Cs-135, Se-79, and Zr-93—affect the long-term performance of the geological barrier.

The results indicate that the nuclide breakthrough time (T_t) ranges from 3600 to 12,000 years, with the maximum value being 3.3 times greater than the minimum. Similarly, the maximum and minimum values of the maximum nuclide breakthrough concentration (C_{\max}) are 4.26×10^{-4} mSv/a and 2.64×10^{-5} mSv/a, respectively, with the former being 16.1 times higher than the latter. These significant differences underscore the significant effect of the uncertainty in 3D DFM models on the long-term performance of geological barriers. After the failure of the waste tank (1000 years), nuclides are predicted to reach the outlet boundary approximately 6480 years later. Subsequently, the individual effective dose in the biosphere initially increases and then decreases. It peaks at $C_{\max} = 4.26 \times 10^{-4}$ mSv/a around 350,000 years, which remains below the critical dose of 0.01 mSv/a. These findings suggest the modeling workflow considering a 3D discrete fracture–matrix system can provide a reference for the design of the potential geological disposal of high-level radioactive waste. Furthermore, the sensitivity analysis results concerning nuclide migration in discrete fractured granite can enhance the simulation and prediction accuracy for risk evaluation of HLW disposal.

In this study, we present an uncertainty analysis of field-data-based randomly distributed fracture network structures on long-term nuclide migration in granite barriers considering a 3D DFM model, which is crucial for assessing and managing the risks associated with nuclear waste disposal. The uncertainty analysis is conducted in two steps. First, a large number of (60) Monte Carlo simulations are conducted to provide statistically representative results on the nuclide migration processes using randomly generalized multiple parameter distributions. Secondly, based on these results, the variability in the breakthrough curves, times, and concentrations caused by the inherent uncertainty associated with the randomly distributed fracture network structures is systematically investigated. By quantifying and addressing the uncertainty of fracture network structures, the limitations of the models and results can be better understood, and the results can provide more reliable and robust assessments of the long-term performance of granite barriers for nuclear waste repositories. Furthermore, uncertainty and parameter sensitivity analysis for solute or nuclide migration in fractured rock considering a 3D discrete fracture–matrix system can also offer valuable insights into mineral crystallization/dissolution, groundwater contamination remediation, oil/gas and geothermal energy resources for exploitation. For instance, parameters associated with fractured rock aquifers such as the fracture aperture, connectivity, hydraulic conductivity, hydraulic gradient, diffusion coefficient, porosity, dispersivity, and so on are key factors influencing the flow and concentration field in a fracture–matrix system; uncertainty and parameter sensitivity analysis can provide insights into the factors that most strongly influence the fluid flow and solute transport, allowing for the identification of critical parameters and potential pathways for contaminant migration. It may also provide some theoretical guidance for future underground energy developments and environmental assessments in fracture reservoirs.

In the future, a better representation of the 3D DFM models that incorporates a more realistic geometric structure can provide valuable insights into the behavior of fractured rocks under different conditions. Meanwhile, increasingly available field data can be obtained from ongoing repository construction work, or that under planning, of underground research laboratories (URLs), and therefore a more comprehensive and convergent understanding of the long-term performance of HLW repositories for post-closure safety analyses can be obtained based on the simulation methods. Thus, more systematic uncertainty and parameter sensitivity analysis algorithms are necessary to optimize the design and manage

the risks associated with long-term nuclide migration in geological repositories, ensuring the safe and sustainable disposal of nuclear waste.

Author Contributions: Methodology, Y.H.; software, W.X.; formal analysis, Y.H. and S.H.; data curation, R.C.; writing—original draft preparation, Y.H.; writing—review and editing, W.X.; supervision, L.Z. and Z.D.; funding acquisition, Y.H. and W.X. All authors have read and agreed to the published version of the manuscript.

Funding: This research was funded by the National Natural Science Foundation of China, grant numbers 42302303 and 42277128; the Zhejiang Provincial Natural Science Foundation of China, grant number ZCLQ24D0201; and the Foundation of Key Laboratory of Soft Soils and Geoenvironmental Engineering (Zhejiang University), Ministry of Education, grant number 2022P07.

Data Availability Statement: Data is contained within the article.

Acknowledgments: The authors thank the reviewers and editors for their useful comments, which led to improvement of the content of the paper.

Conflicts of Interest: The authors declare no conflicts of interest.

References

1. El-Emam, R.S.; Ozcan, H.; Zamfirescu, C. Updates on promising thermochemical cycles for clean hydrogen production using nuclear energy. *J. Clean. Prod.* **2020**, *262*, 121424. [[CrossRef](#)]
2. Azam, A.; Rafiq, M.; Shafique, M.; Zhang, H.; Yuan, J. Analyzing the effect of natural gas, nuclear energy and renewable energy on GDP and carbon emissions: A multi-variate panel data analysis. *Energy* **2021**, *219*, 119592. [[CrossRef](#)]
3. Tsang, C.; Neretnieks, I.; Tsang, Y. Hydrologic issues associated with nuclear waste repositories. *Water Resour. Res.* **2015**, *51*, 6923–6972. [[CrossRef](#)]
4. Wang, J.; Chen, L.; Su, R.; Zhao, X. The Beishan underground research laboratory for geological disposal of high-level radioactive waste in China: Planning, site selection, site characterization and in situ tests. *J. Rock Mech. Geotech. Eng.* **2018**, *10*, 411–435. [[CrossRef](#)]
5. Liu, Y.; Ma, L.; Ke, D.; Cao, S.; Xie, J.; Zhao, X.; Chen, L.; Zhang, P. Design and validation of the THMC China-Mock-Up test on buffer material for HLW disposal. *J. Rock Mech. Geotech. Eng.* **2014**, *6*, 119–125. [[CrossRef](#)]
6. Xu, W.; Hu, Y.; Chen, Y.; Zhan, L.; Chen, R.; Li, J.; Zhuang, D.; Li, Q.; Li, K. Hyper-gravity experiment of solute transport in fractured rock and evaluation method for long-term barrier performance. *Rock Mech. Bull.* **2023**, *2*, 100042. [[CrossRef](#)]
7. Zhao, Z.; Chen, S.; Zhang, J.; Chen, J.; Wu, Y. In-situ tracer test in fractured rocks for nuclear waste repository. *Earth-Sci. Rev.* **2024**, *250*, 104683. [[CrossRef](#)]
8. Andersson, P.; Wass, E.; Johansson, H.; Skarnemark, G.; Skålberg, M. *Äspö Hard Rock Laboratory, TRUE 1st Tracer Test Programme, Tracer Tests with Sorbing Tracers, STT-1b, Experimental Description and Preliminary Evaluation*; IPR-99-12; Swedish Nuclear Fuel and Waste Management Co.: Stockholm, Sweden, 1999.
9. Lindquist, A. *Forsmark Site Investigation: Confirmatory Hydraulic Interference Test and Tracer Test at Drill Site 2*; Svensk Kärnbränslehantering (SKB): Stockholm, Sweden, 2008.
10. Soler, J.M.; Landa, J.; Havlova, V.; Tachi, Y.; Ebina, T.; Sardini, P.; Siitari-Kauppi, M.; Eikenberg, J.; Martin, A.J. Comparative modeling of an in situ diffusion experiment in granite at the Grimsel Test Site. *J. Contam. Hydrol.* **2015**, *179*, 89–101. [[CrossRef](#)] [[PubMed](#)]
11. Tanaka, Y.; Kinashi, K.; Kono, K.; Sakai, W.; Tsutsumi, N. Electron spin resonance and photoelectron yield spectroscopic studies for photocarrier behavior in photorefractive polymeric composites. *Org. Electron.* **2019**, *68*, 248–255. [[CrossRef](#)]
12. Dai, Z.; Wolfsberg, A.; Lu, Z.; Deng, H. Scale dependence of sorption coefficients for contaminant transport in saturated fractured rock. *Geophys Res. Lett.* **2009**, *36*, 1. [[CrossRef](#)]
13. Jia, S.; Dai, Z.; Yang, Z.; Du, Z.; Zhang, X.; Ershadnia, R.; Soltanian, M.R. Uncertainty quantification of radionuclide migration in fractured granite. *J. Clean. Prod.* **2022**, *366*, 132944. [[CrossRef](#)]
14. Ma, F.; Zhang, X.; Zhan, C.; Chen, W.; Qi, L.; Dai, Z. Upscaling of Se(IV) sorption coefficients with hierarchical mineral characterization in multi-scale fractured granite. *Stoch. Environ. Res. Risk Assess.* **2023**, *37*, 877–887. [[CrossRef](#)]
15. Hyman, J.D.; Painter, S.L.; Viswanathan, H.; Makedonska, N.; Karra, S. Influence of injection mode on transport properties in kilometer-scale three-dimensional discrete fracture networks. *Water Resour. Res.* **2015**, *51*, 7289–7308. [[CrossRef](#)]
16. Cao, X.; Hu, L.; Wang, J.; Wang, J. Radionuclide transport model for risk evaluation of high-level radioactive waste in Northwestern China. *Hum. Ecol. Risk Assess. Int. J.* **2017**, *23*, 2017–2032. [[CrossRef](#)]
17. Wei, Y.; Dong, Y.; Yeh, T.J.; Li, X.; Wang, L.; Zha, Y. Assessment of uncertainty in discrete fracture network modeling using probabilistic distribution method. *Water Sci. Technol.* **2017**, *76*, 2802–2815. [[CrossRef](#)] [[PubMed](#)]
18. Ma, G.; Li, T.; Wang, Y.; Chen, Y. Numerical simulations of nuclide migration in highly fractured rock masses by the unified pipe-network method. *Comput. Geotech.* **2019**, *111*, 261–276. [[CrossRef](#)]

19. Winberg, A.; Andersson, P.; Hermanson, J.; Byegaard, J.; Cvetkovic, V.; Birgersson, L. *Äspö Hard Rock Laboratory. Final Report of the First Stage of the Tracer Retention Understanding Experiments*; Swedish Nuclear Fuel and Waste Management Co.: Stockholm, Sweden, 2000.
20. Elert, M.; Svensson, H. *Evaluation of Modelling of the TRUE-1 Radially Converging Tests with Sorbing Tracers. The Äspö Task Force on Modelling of Groundwater Flow and Transport of Solutes. Tasks 4E and 4F*; Swedish Nuclear Fuel and Waste Management Co.: Stockholm, Sweden, 2001.
21. Lindquist, A.; Hjerne, C.; Nordqvist, R.; Wass, E. *Forsmark Site Investigation: Large-Scale Confirmatory Multiple-Hole Tracer Test*; Svensk kärnbränslehantering (SKB): Stockholm, Sweden, 2008.
22. Ikonen, J.; Sardini, P.; Jokelainen, L.; Siitari-Kauppi, M.; Martin, A.; Eikenberg, J. The tritiated water and iodine migration in situ in Grimsel granodiorite. Part I: Determination of the diffusion profiles. *J. Radioanal. Nucl. Chem.* **2016**, *310*, 1041–1048. [[CrossRef](#)]
23. Ling, H.; Wang, J.; Chen, W. Simulation study on retardation of nuclides by granite geological barriers. *China Sciencepaper* **2017**, *12*, p2507.
24. Duan, X.; Niu, S.; Wang, C.; Wang, J.; Zhou, Z.; Ling, H.; Tang, Z.; Li, N. Safety evaluation study on the geological disposal of high-level radioactive waste: A case study of Beishan, Gansu province. *China Min. Mag.* **2021**, *30*, 56–63.
25. Pavičić, I.; Duić, Ž.; Vrbaški, A.; Dragičević, I. Fractal Characterization of Multiscale Fracture Network Distribution in Dolomites: Outcrop Analogue of Subsurface Reservoirs. *Fractal Fract.* **2023**, *7*, 676. [[CrossRef](#)]
26. Huang, N.; Liu, R.; Jiang, Y.; Cheng, Y. Development and application of three-dimensional discrete fracture network modeling approach for fluid flow in fractured rock masses. *J. Nat. Gas Sci. Eng.* **2021**, *91*, 103957. [[CrossRef](#)]
27. Zou, L.; Cvetkovic, V. Inference of Transmissivity in Crystalline Rock Using Flow Logs Under Steady-State Pumping: Impact of Multiscale Heterogeneity. *Water Resour. Res.* **2020**, *56*, e2020WR027254. [[CrossRef](#)]
28. Basirat, R.; Goshtasbi, K.; Ahmadi, M. Determination of the Fractal Dimension of the Fracture Network System Using Image Processing Technique. *Fractal Fract.* **2019**, *3*, 17. [[CrossRef](#)]
29. Nykyri, M.; Nordman, H.; Marcos, N.; Löfman, J.; Poteri, A.; Hautojärvi, A. Radionuclide Release and Transport. RNT-2008. 2008. Available online: <https://cris.vtt.fi/en/publications/radionuclide-release-and-transport-rnt-2008> (accessed on 1 April 2024).
30. Hyman, J.D.; Karra, S.; Makedonska, N.; Gable, C.W.; Painter, S.L.; Viswanathan, H.S. dfnWorks: A discrete fracture network framework for modeling subsurface flow and transport. *Comput. Geosci.* **2015**, *84*, 10–19. [[CrossRef](#)]
31. Neretnieks, I. Diffusion in the rock matrix: An important factor in radionuclide retardation? *J. Geophys. Res.* **1980**, *85*, 4379–4397. [[CrossRef](#)]
32. Tang, D.H.; Frind, E.O.; Sudicky, E.A. Contaminant transport in fractured porous media: Analytical solution for a single fracture. *Water Resour. Res.* **1981**, *17*, 555–564. [[CrossRef](#)]
33. Sudicky, E.A.; Frind, E.O. Contaminant transport in fractured porous media: Analytical solutions for a system of parallel fractures. *Water Resour. Res.* **1982**, *18*, 1634–1642. [[CrossRef](#)]
34. Rejeb, A.; Bruel, D. Hydromechanical effects of shaft sinking at the Sellafield site. *Int. J. Rock Mech. Min. Sci.* **2001**, *38*, 17–29. [[CrossRef](#)]
35. Ahmed, R.; Edwards, M.G.; Lamine, S.; Huisman, B.A.H.; Pal, M. Three-dimensional control-volume distributed multi-point flux approximation coupled with a lower-dimensional surface fracture model. *J. Comput. Phys.* **2015**, *303*, 470–497. [[CrossRef](#)]
36. Keilegavlen, E.; Berge, R.; Fumagalli, A.; Starnoni, M.; Stefansson, I.; Varela, J.; Berre, I. PorePy: An open-source software for simulation of multiphysics processes in fractured porous media. *Computat. Geosci.* **2021**, *25*, 243–265. [[CrossRef](#)]
37. Hu, Y.; Xu, W.; Zhan, L.; Zou, L.; Chen, Y. Modeling of solute transport in a fracture-matrix system with a three-dimensional discrete fracture network. *J. Hydrol.* **2022**, *605*, 127333. [[CrossRef](#)]
38. Ben Abdelghani, F.; Aubertin, M.; Simon, R.; Therrien, R. Numerical simulations of water flow and contaminants transport near mining wastes disposed in a fractured rock mass. *Int. J. Min. Sci. Technol.* **2015**, *25*, 37–45. [[CrossRef](#)]
39. Hyman, J.D.; Sweeney, M.R.; Gable, C.W.; Svyatsky, D.; Lipnikov, K.; David Moulton, J. Flow and transport in three-dimensional discrete fracture matrix models using mimetic finite difference on a conforming multi-dimensional mesh. *J. Comput. Phys.* **2022**, *466*, 111396. [[CrossRef](#)]
40. Ma, L.; Gao, D.; Qian, J.; Han, D.; Xing, K.; Ma, H.; Deng, Y. Multiscale fractures integrated equivalent porous media method for simulating flow and solute transport in fracture-matrix system. *J. Hydrol.* **2023**, *617*, 128845. [[CrossRef](#)]
41. Chen, W. Study of System Analysis Method for Geological Repository of High Level Radioactive Waste-Taking the Beishan Granite Site as an Example. Ph.D. Thesis, Beijing Research Institute of Uranium Geology, Beijing, China, 2008.
42. Guo, L.; Li, X.; Zhou, Y.; Zhang, Y. Generation and verification of three-dimensional network of fractured rock masses stochastic discontinuities based on digitalization. *Environ. Earth Sci.* **2015**, *73*, 7075–7088. [[CrossRef](#)]
43. Guo, L.; Wu, L.; Zhang, J.; Liao, M.; Ji, Y. Identification of homogeneous region boundaries of fractured rock masses in candidate sites for Chinese HLW repository. *Bull. Eng. Geol. Environ.* **2020**, *79*, 4221–4243. [[CrossRef](#)]
44. Xu, W.; Zhang, Y.; Li, X.; Wang, X.; Ma, F.; Zhao, J.; Zhang, Y. Extraction and statistics of discontinuity orientation and trace length from typical fractured rock mass: A case study of the Xinchang underground research laboratory site, China. *Eng. Geol.* **2020**, *269*, 105553. [[CrossRef](#)]
45. Bonnet, E.; Bour, O.; Odling, N.E.; Davy, P.; Main, I.; Cowie, P.; Berkowitz, B. Scaling of fracture systems in geological media. *Rev. Geophys* **2001**, *39*, 347–383. [[CrossRef](#)]

46. Davy, P.; Le Goc, R.; Darcel, C.; Bour, O.; de Dreuzy, J.R.; Munier, R. A likely universal model of fracture scaling and its consequence for crustal hydromechanics. *J. Geophys. Res. Solid Earth* **2010**, *115*, 2009JB007043. [[CrossRef](#)]
47. Afshari Moein, M.J.; Valley, B.; Evans, K.F. Scaling of fracture patterns in three deep boreholes and implications for constraining fractal discrete fracture network models. *Rock Mech. Rock Eng.* **2019**, *52*, 1723–1743. [[CrossRef](#)]
48. Lei, G. Study on Rockmass Joints Geometric Feature and Three-Dimension Network Simulation. Ph.D. Thesis, Chongqing University, Chongqing, China, 2015.
49. Li, M. Research and Application of Rock Mass Structure Plane Features of Xinchang Section in Beishan Preselected Area of Gansu. Master's Thesis, China University of Geosciences (Beijing), Beijing, China, 2020.
50. Zhan, L.; Hu, Y.; Zou, L.; Xu, W.; Ye, Z.; Chen, R.; Zhuang, D.; Li, J.; Chen, Y. Effects of multiscale heterogeneity on transport in three-dimensional fractured porous rock with a rough-walled fracture network. *Comput. Geotech.* **2022**, *148*, 104836. [[CrossRef](#)]
51. Hyman, J.D.; Aldrich, G.; Viswanathan, H.; Makedonska, N.; Karra, S. Fracture size and transmissivity correlations: Implications for transport simulations in sparse three-dimensional discrete fracture networks following a truncated power law distribution of fracture size. *Water Resour. Res.* **2016**, *52*, 6472–6489. [[CrossRef](#)]
52. Kolditz, O.; Bauer, S.; Bilke, L.; Böttcher, N.; Delfs, J.O.; Fischer, T.; Görke, U.J.; Kalbacher, T.; Kosakowski, G.; McDermott, C.I.; et al. OpenGeoSys: An open-source initiative for numerical simulation of thermo-hydro-mechanical/chemical (THM/C) processes in porous media. *Environ. Earth Sci.* **2012**, *67*, 589–599. [[CrossRef](#)]
53. Chen, C.; Binder, M.; Oppelt, L.; Hu, Y.; Engelmann, C.; Arab, A.; Xu, W.; Scheytt, T.; Nagel, T. Modeling of heat and solute transport in a fracture-matrix mine thermal energy storage system and energy storage performance evaluation. *J. Hydrol.* **2024**, *636*, 131335. [[CrossRef](#)]
54. JNC-H. *JNC-H12, 2000: Project to Establish the Scientific and Technical Basis for HLW Disposal in Japan, Supporting Report 3: Safety Assessment of the Geological Disposal System*; Japan Nuclear Cycle Development Institute: Tōkai, Japan, 2000.
55. Ling, H. Post-Closure Safety Assessment for High-level Radioactive Waste Repository in Beishan, China. Ph.D. Thesis, Beijing Research Institute of Uranium Geology, Beijing, China, 2018.

Disclaimer/Publisher's Note: The statements, opinions and data contained in all publications are solely those of the individual author(s) and contributor(s) and not of MDPI and/or the editor(s). MDPI and/or the editor(s) disclaim responsibility for any injury to people or property resulting from any ideas, methods, instructions or products referred to in the content.